10^{th} International Conference on Fracture Mechanics of Concrete and Concrete Structures
FraMCoS-X
G. Pijaudier-Cabot, P. Grassl and C. La Borderie (Eds)
https://doi.org/10.21012/FC10.235586

A FIRST APPROACH TO COMPARING COHESIVE TRACTION-SEPARATION LAWS FOR CONCRETE

JAIME PLANAS*, BEATRIZ SANZ† AND JOSE M. SANCHO‡

*Universidad Politécnica de Madrid
ETS de Ingenieros de Caminos, Canales y Puertos, Profesor Aranguren 3, 28040 Madrid, Spain
e-mail: jaime.planas@upm.es

†Universidad Politécnica de Madrid
ETS de Ingenieros de Caminos, Canales y Puertos, Profesor Aranguren 3, 28040 Madrid, Spain
e-mail: beatriz.sanz@upm.es

‡Universidad Politécnica de Madrid
ETS de Arquitectura, Avda. Juan Herrera 3, 28040 Madrid, Spain
e-mail: jose.sancho@upm.es

Key words: Cohesive Crack,Embedded Crack, Traction-Separation Laws

Abstract. In the already vast literature dealing with numerical simulations of fracture of concrete elements or structures, a large number of papers deal with cohesive traction-separation laws. However, in many instances, this appears to be a secondary aspect of the published studies, the principal one being the variant of the numerical algorithm being presented in the research. This makes difficult to compare the various available formulations for the vectorial traction-separation law ($\mathbf{t}$–$\mathbf{w}$ law). The present work aims at initiating a systematic comparison between the $\mathbf{t}$–$\mathbf{w}$ laws, and this is done comparing a subset of the possible formulations using exactly the same numerical algorithms. The analysis is restricted, in this contribution, to damage-based models in the tensile zone (positive normal components of the traction and the crack displacement vectors). All the models use the same uniaxial softening function and the emphasis is on the vectorial character of the $\mathbf{t}$–$\mathbf{w}$ law, namely, on the influence of (1) the lack of coaxiality of $\mathbf{t}$ and $\mathbf{w}$; (2) the shape of the damage criterion in the traction space; and (3) the influence of the ratio of fracture energies in pure modes I and II. The simulations have been carried out within the finite element framework COFE (Continuum Oriented Finite Element), which implements elements with an embedded adaptable crack to reproduce fracture of concrete as well as a smeared version that, essentially, unifies the numerical algorithms of both approaches.

1 INTRODUCTION

In the already vast literature dealing with cohesive cracking in concrete and other quasibrittle materials since Hillerborg introduced the "fictitious crack model" in the mid 1970s [1], the numerical techniques aimed at the application of cohesive models to structural analysis are predominant, especially along the last two decades. An essential ingredient of such numerical models is the behavior of the cohesive crack itself, characterized by a law relating the traction vector transferred across the crack faces $\mathbf{t}$ to the relative displacement vector between those faces $\mathbf{w}$, usually abbreviated to *traction-separation law* of the cohesive crack (or $\mathbf{t}$-$\mathbf{w}$ law). Unfortunately, most of the available publications are more focused on the computational technologies than in the cohesive behavior itself and it is difficult to draw general conclusions about the suitability of the various traction-separation laws because few studies are available that compare them without concurrent substantial changes in numerical methodologies and algorithms.

The present work reports the initial results of a systematic research on the essential conditions that a traction-separation law should fulfill to guarantee that it does not carry any deleterious collateral effects on the numerical calculations. The paper is organized as follows: A brief account is given in Sec. 2, which is followed, in Sec 3, by the description of a family of damage-based models which includes most of the models of that kind that can be found in the literature; Sec. 4 reports results of a numerical study on the effect of the two principal parameters of the family of models in a paradigmatic case; Sec. 5 closes the paper with the main conclusions of the work.

2 BACKGROUND

2.1 Cohesive crack basics

This work focuses on the generalization of the cohesive model proposed initially for concrete cracking in Mode I (pure opening) by Hillerborg and co-workers, which has been extensively used for that material as well as many other quasibrittle materials [1–5]. In essence, the model assumes that the material outside the fracture surfaces remains in linear-elastic regime at all times; when, a a point, the maximum principal stress σ_1 reaches the tensile strength f_t of the material, a crack forms at that point which is locally perpendicular to the maximum principal stress direction. When the crack opening w of that crack at that point increases monotonically in pure Mode I, the model assumes that the traction vector over the crack faces is normal to the crack and its magnitude σ is given by a function of w which is a material property; thus, we write;

$$\sigma = f(w) \tag{1}$$

For general purpose computations, in which no pure opening mode can be anticipated, a vectorial relationship is required relating the traction vector $\mathbf{t}$ to the separation vector $\mathbf{w}$ defined as the displacement of one face of the crack with respect to the other (which is taken as a reference. $f(w)$ is called the softening curve in pure Mode I. It is schematically represented in Fig. 1 and is one of the fundamental ingredients of the cohesive behavior, but not the only one, because, in general, cracks do not evolve in pure Mode I.

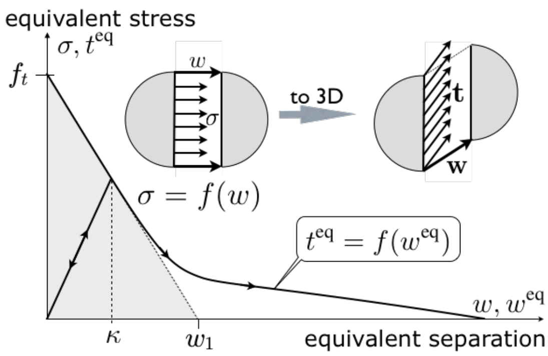

Figure 1: Cohesive crack model in pure opening mode (Mode I). The equivalent values for the traction ($t^{\rm eq}$) and the separation ($w^{\rm eq}$) are defined in Sec. 3 for the models under scrutiny.

2.2 Traction separation laws

In the published works, three families of traction-separation laws can be identified:

(**1**) Elastic (reversible) models in which the $\mathbf{t}$-$\mathbf{w}$ law derives from a potential function and, thus, cannot correctly describe unloading processes (see [6] for a recent review of such kind of models).

(**2**) Elasto-plastic models in which the formulation parallels that of classical continuum elastoplasticty, but vectorial relationships between $\mathbf{t}$ and $\mathbf{w}$ are set instead of $\boldsymbol{\sigma}$ and $\boldsymbol{\epsilon}$ [7–13]; since the stiffness of the crack just after initiation is nominally infinite, in the limit its behavior should be rigid-plastic, and these models are characterized by a very stiff unloading response.

(**3**) Damage-based models obtained by exporting classical continuum damage approaches to vectorial, rather than tensorial, relationships, characterized by displaying linear unloading to the origin [14–24].

Obviously, models exist that combine some of the characteristics of the aforementioned ones, an a few more that do not fit into any of those categories. Among the last-mentioned are the pioneering works of Rots and others [25,26] in which the the formulation is strictly tangent and so is based on differential relationships of the hypoelastic type $\dot{\mathbf{t}} = \mathbf{K}\dot{\mathbf{w}}$, where $\mathbf{K}$ is a tangent stiffness tensor depending on other state variables. The essential of these models was later reformulated in secant form [11,12,27,28]; versions of such kind can be found in various commercial finite element programs.

2.3 About traction-separation coaxiality

There is a good reason to believe that, in this kind of models, the vectors $\mathbf{t}$ and $\mathbf{w}$ must be coaxial (parallels): this is a necessary condition for the fracture power per unit surface $\mathbf{t}\cdot\dot{\mathbf{w}}$ be frame independent [29]. This is due to a lack of rotational equilibrium in the system of forces acting on the crack faces [30], as depicted in Fig. 2. This fundamental facts attracted little attention until relatively recent times, and most existing models allow non coaxial traction-separation laws, and so does the family of models that we consider in the following.

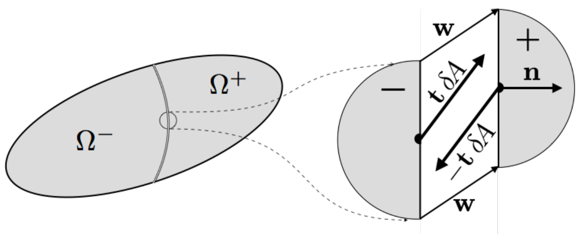

Figure 2: Resultant forces on the faces of the cracks in an elemental ball diagonally split by the crack; δA is the area of the crack disk (adapted from [31]).

3 A DAMAGE-BASED FAMILY OF TRACTION-SEPARATION LAWS

3.1 Basic formulation

The model is developed in the framework of constitutive equations with internal variables (see, e.g., [32]) in which the usual tensorial variables stress and strain are replaced by the vectorial variables $\mathbf{t}$-$\mathbf{w}$. The simplest model assumes a single monotonically increasing internal variable κ, and we look for a function $\mathbf{t} = \mathbf{t}(\mathbf{w}, \kappa; \mathbf{n})$ that includes a parametric dependence on the unit normal to the crack faces $\mathbf{n}$. Assuming that the Helmholtz free energy per unit area is a function $\psi(\mathbf{w}, \kappa; \mathbf{n})$ depending quadratically on $\mathbf{w}$, and assuming, furthermore, material isotropy, we get, following a procedure similar to that followed by Jirásek in [10] and [33], the following expression for the cohesive traction:

$$\mathbf{t} = k_n(\kappa) w_n \mathbf{n} + k_s(\kappa)\mathbf{w}_s$$

where $k_n(\kappa)$ and $k_s(\kappa)$ are, respectively, the normal and shear stiffnesses which must be decreasing functions of κ to satisfy the principle of universal dissipation. In the previous expressions, $w_n\mathbf{n}$ and $\mathbf{w}_s$ are the vectorial projections of $\mathbf{w}$, respectively, on the normal and on the plane of the crack; their analytical expressions are

$$w_n := \mathbf{w}\cdot\mathbf{n}\,, \quad , \quad \mathbf{w}_s := \mathbf{w} - w_n\mathbf{n}.$$

To simplify the model, it is usually assumed that the ratio of the stiffnesses is constant [10, 14, 33], and write $k_s(\kappa) = \beta^2 k_n(\kappa)$, $\beta = \text{const} > 0$, to get

$$\mathbf{t} = k_n(\kappa)(w_n\mathbf{n} + \beta^2\mathbf{w}_s)\,. \tag{2}$$

To complete the model, we need to establish the laws for damage growth, and the function for the normal stiffness. Thus, we first assume that there exist: (1) a scalar function of the separation vector that we call *equivalent separation* $w^{\text{eq}}(\mathbf{w})$, and (2) a damage criterion stating that κ is the historical maximum of w^{eq}, which reduce to any of the equivalent conditions

$$w^{\text{eq}}(\mathbf{w}) \le \kappa \quad \Leftrightarrow \quad \kappa = \max[\, w^{\text{eq}}(\mathbf{w})\,]\,. \tag{3}$$

If we choose function $w^{\text{eq}}(\mathbf{w})$ so that in pure Mode I its value coincides with the normal separation, i.e., satisfying

$$w^{\text{eq}}(w\mathbf{n}) = w\,, \tag{4}$$

and we further impose the condition that in Mode I the relation between the stress and the separation is given by the softening function (1), it is easy to reduce expressions (2) and (3) to

$$\mathbf{t} = \frac{f(\kappa)}{\kappa}(w_n\mathbf{n} + \beta^2\mathbf{w}_s),\ \kappa = \max[w^{\text{eq}}(\mathbf{w})], \tag{5}$$

since, then, for pure monotonic opening mode we have $\kappa = w_n = w,\ \mathbf{w}_s = \mathbf{0}$ and the foregoing equation trivially reduces to $\mathbf{t} = \sigma\mathbf{n} = f(w)\mathbf{n}$, which is the vectorial form of Eq. (1).

One of the simplest expressions for w^{eq} satisfying condition (4) —and the one investigated in the remaining part of the paper— is the following:

$$w^{\text{eq}} := \sqrt{w_n^2 + \frac{\beta^2}{\alpha^2}w_s^2}\,, \tag{6}$$

where $w_s := |\mathbf{w}_s| = \sqrt{\mathbf{w}_s\cdot\mathbf{w}_s}$ is the magnitude of the shear component, and α is a further material constant which meaning is disclosed next.

3.2 Fracture energies

Although, in practice, it is impossible to initiate cracking of the bulk material in mixed mode, because the most unfavorable orientation for cracking always coincide with a principal stress plane, we can, based on the foregoing equations, compute the *theoretical* value of the fracture energy along any assumed path in the separation space. In particular, we assume a proportional separation path in which $\mathbf{w} = w_n\mathbf{n} + mw_n\mathbf{e}_s$, where $\mathbf{e}_s$ is a constant unit vector perpendicular to $\mathbf{n}$ and $m := w_s/w_n$ is the *constant* ratio between the shear and the normal components of the separation vector. In this case we have, substituting in (6) and assuming that w_n increases monotonically,

$$\kappa = \sqrt{\alpha^2 + \beta^2 m^2}\,\frac{w_n}{\alpha} \Rightarrow w_n = \frac{\alpha\kappa}{\sqrt{\alpha^2 + \beta^2 m^2}}$$

and the fracture energy for final fracture is

$$\begin{aligned} G_F(m) &= \int_0^\infty \mathbf{t}\cdot\frac{\partial\mathbf{w}}{\partial w_n}dw_n \\ &= \frac{\alpha^2(1+\beta^2m^2)}{\alpha^2+\beta^2m^2}\int_0^\infty f(\kappa)d\kappa \end{aligned}$$

and since the last integral equals the Mode I fracture energy, we have that the *theoretical* fracture energies in mixed mode with proportional separation path, and in Mode II are, respectively,

$$G_F(m) = \frac{\alpha^2(1+\beta^2m^2)}{\alpha^2+\beta^2m^2}G_F^I\,, \tag{7}$$

$$G_F^{II} = \alpha^2 G_f^I\,, \tag{8}$$

where the last expression is obtained as the limit of the first for $m \to \infty$.

It may be noticed that for $\alpha = 1$, the fracture energy is fully path-independent for any value of β.

Most of the published models can be rewritten as particular cases of the foregoing model. Most of them correspond to cases with coaxial traction-separation and path-independent fracture energy ($\alpha = \beta = 1$) [20–23], some imply central forces ($\beta = 1$) [17], some enjoy pah independent fracture energy ($\alpha = 1$) [14–16], and the models in [18,19,24] depend on a single parameter implying a functional relationship between α y β.

3.3 Damage criteria

The damage criterion expressed in equivalent separation is the inequality of equation $(5)_1$, with w^{eq} given by (6). Its graphical representation in a plane w_n-w_s shows that the instantaneous elastic domain is a quarter of an ellipse with semi-axes κ and $\alpha\kappa/\beta$ (Fig. 3a). The elastic domain homogeneously expands with increasing damage $\boldsymbol{\kappa}$. Since the initial elastic domain collapses into the origin, the crack initiation condition is better described in the traction space which is obtained as described next.

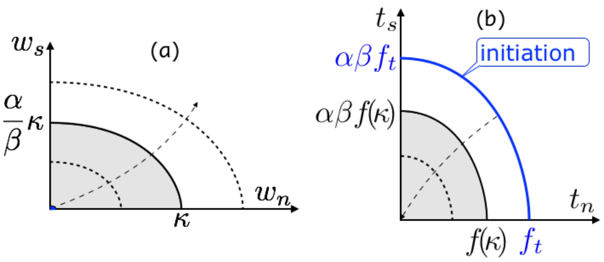

Figure 3: Damage criteria and their evolution: (a) in the separation space, and (b) in the traction space. The shaded quarter-ellipses are the instantaneous elastic domains, which expand homogeneously in (a) and shrink in (b).

We solve from Eq. $(5)_1$ for the normal and shear components of $\mathbf{w}$ as functions of the corresponding components of $\mathbf{t}$ and insert the result in the criterion expressed in separation; after simplifying an reordering we get the equation of the elastic domain in the traction space as

$$t^{\text{eq}} := \sqrt{t_n^2 + \frac{t_s^2}{\alpha^2\beta^2}} \leq f(\kappa) \tag{9}$$

which shows that the elastic domains are, again, similar quarter-ellipses with center at the origin an semi-axes $f(\kappa)$ and $\alpha\beta f(\kappa)$ as shown in Fig. 3b. Also shown in this figure is the crack initiation criterion (thick blue curve).

Turning now to the crack initiation in an initially uncracked continuum, Fig. 4 shows Mohr's circles for simple tension an pure shear for which the experience shows that cracks form perpendicular to the principal direction of maximum tension. Thus, the crack initiation criterion (blue line in the figure) must be tangent to Mohr's circles at their rightmost point, and *external* to the Mohr's circles anywhere else, which implies that α and β must satisfy $\alpha\beta > 1$.

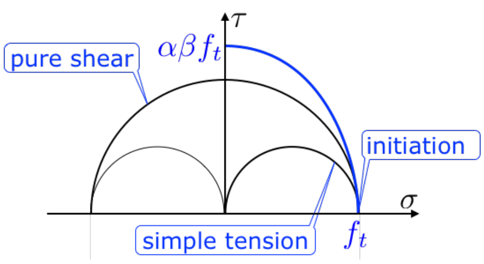

Figure 4: Mohr's circles at crack initiation in an uncracked continuum point for simple tension an pure shear.

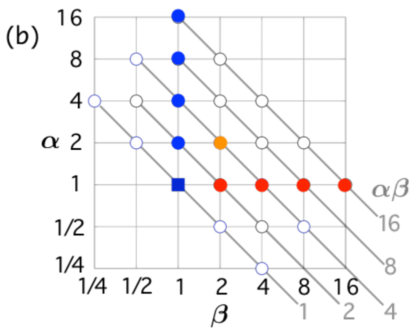

Figure 5: Combinations of α and β explored in the paper.

Figure 5 displays a bilogarithmic β-α diagram showing the combinations of values that are investigated in this paper, all satisfying the previous condition.

4 EFFECT OF PARAMETERS α AND β

4.1 Numerical method

Figure 6 shows the main ingredients of the numerical model, which coincide, in essence with those presented in [21], except that vectors $\mathbf{t}$ y $\mathbf{w}$ do not need to be parallel (they are not if $\beta \neq 1$) and the equivalent separation does not need, either, to be equal to the magnitude of $\mathbf{w}$ (it is not if $\alpha \neq \beta$).

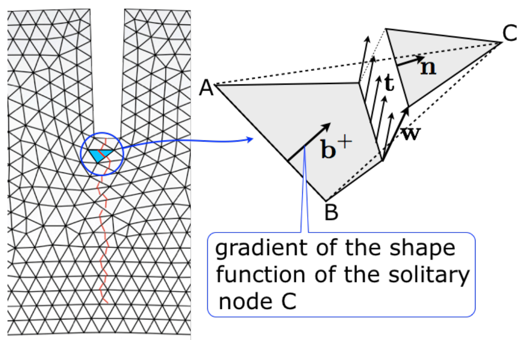

Figure 6: Cohesive crack embedded in a finite element (adapted from [34]).

Otherwise, the element type (constant strain triangles), the crack kinematics (strong discontinuity), and the remaining characteristics are identical to those described in [21]. Among those characteristics, the following are worth being recalled: (1) the crack is required to satisfy local equilibrium, which implies that its exact position in the element is not required; (2) the computations are strictly local, i.e., no crack tracking algorithm is used, the orientation of the crack in the element and the corresponding solitary node are determined based only of the current nodal displacements in the corresponding element; however, two strictly numerical expedients are used to avoid crack locking: (3) the initial elastic stiffness matrix is used for the element throughout the computation; and (4) the crack in the element is allowed to reorient itself following the principal stress rotations while its equivalent crack opening is small compared to w_1 defined in Fig. 1 (this is called *limited crack adaptability*).

Feature (3) implies a large number of iterations (but these are very fast because back substitution is only required), which turns out to be a virtue when combined with feature (4) since the cracks are given more opportunities to adopt the right orientation (or even get closed), while seeking for convergence, in a kind of self-annealing process.

With that procedure and the new equations for the traction-separation law, an extensive parametric study is under way to ascertain the influence of the parameters α and β. The first step consists in simulating highly symmetric problems in which, theoretically, the dominant crack is subjected to pure Mode I, as in the case of a three-point bent beam. In such situation, the results of the simulation should be strictly independent of α and β, since the shear components of the traction and the separation vectors are zero in Mode I. The simulations and their main outcome are described next.

4.2 Three-point bending of a beam

Figure 7 displays the geometry of the beam and the two finite element meshes used in the computations, which were created with the finite element mesher GMSH [35], with default settings.

The softening curve was taken to be linear (dashed straight line in Fig 1) with f_t = 3.0 MPa and $w_1 = 0.030$ mm; the elastic modulus and Poisson's ratio were, respectively set to $E = 30$ GPa and $\nu = 0.17$.

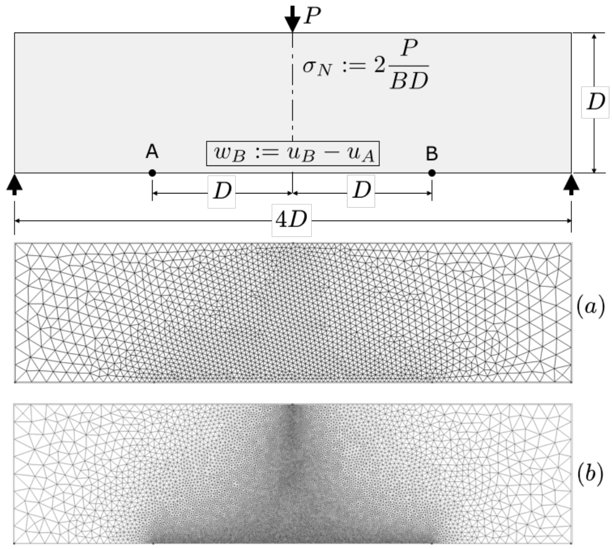

Figure 7: Geometry of the specimen and FE meshes used in the simulations ($D = 100$ mm); coarse mesh (a): 1909 nodes, 3715 elements; fine mesh (b): 13236 nodes, 26315 elements.

The computations were carried out under control of the elongation w_B of the bottom line in the mid-span, as defined in Fig. 7. A total elongation of 0.1 mm was applied in 100 identical steps. Computations have been carried out for the parameter combinations marked with full circles in the diagram of figure 5.

4.3 Numerical results

4.2.1 Coaxial models ($\beta = 1$).

Numerical simulations with $\beta = 1$ ($\mathbf{t}$ and $\mathbf{w}$ coaxials) were carried out for $\alpha = 1, 2, 4, 8, 16$ for both the coarse and the fine mesh. Figure 8 displays the effect of α on the curves load v.s. mid-span elongation, w_B.

The inset in the figure shows a zoom of the area close to the peak in which it is clear that, for each mesh, the effect of α is to increase the load for a given abscissa. The increase is greater when increasing α from 1 to 2, but diminishes for any subsequent doubling and saturates rapidly for $\alpha > 4$ to reach a nearly asymptotic value for $\alpha = 16$.

It can also be noted that for $\alpha = 1$ (path-independent fracture energy), the effect of the mesh is very small, negligible for any practical purpose. However, the effect of increasing α is stronger for the finer mesh, and the question arises about the evolution of the effect upon further refinement.

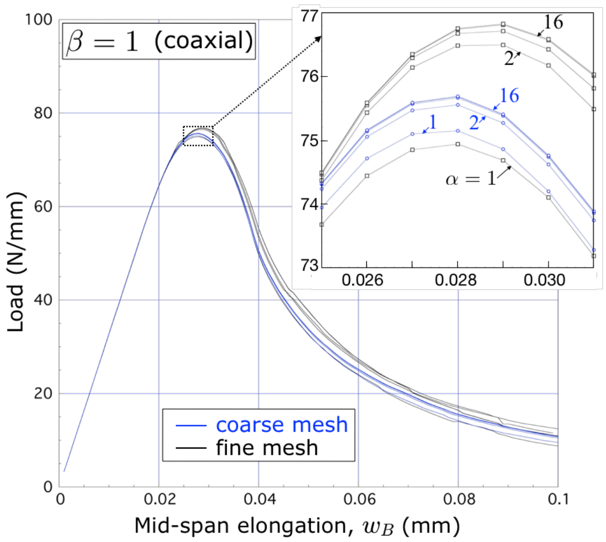

Figure 8: Load (P/B) vs. mid-span elongation (w_B) for $\beta = 1$ and $\alpha = 1, 2, 4, 8, 16$. Curves for coarse mesh in blue, in black for fine mesh.

4.2.2 Non coaxial models ($\beta \neq 1$).

In the set of simulations in which α was kept constant equal to 1 and β was varied from 1 to 32, the trend of the results were found to be completely different from those in the previous paragraph: as can be observed in Fig. 9, the load-w_B curves are drastically different for values of β greater than 2 for the coarser mesh.

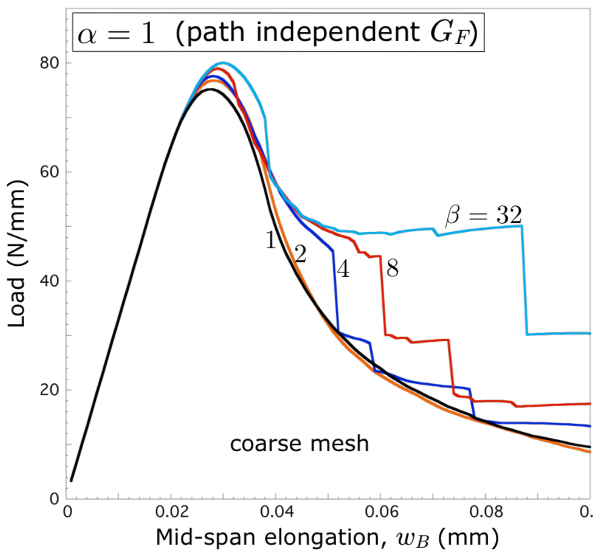

Figure 9: Load (P/B) vs. mid-span elongation (w_B) for $\alpha = 1$ and $\beta = 1, 2, 4, 8, 32$ for the coarse mesh.

In addition to notable increases in the peak load, the lack of coaxiality of **t** y **w** induced by β lead to unstable behavior in the post peak for values of β of 4 or greater.

The situation is even worse for the finer mesh: Figure 10 shows the corresponding curves for that mesh for a few combinations of α and β; the curve for $\alpha = \beta = 1$ computed using the coarse mesh is also included for comparison.

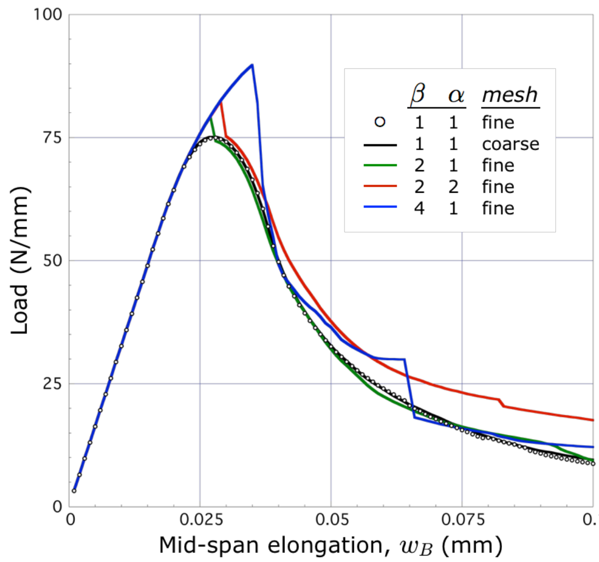

Figure 10: Load (P/B) vs. mid-span elongation (w_B) for various combinations of α, β and mesh.

The curves for $\beta = 1$ are smooth and indistinguishable at the scale of the plot. As β is increased to 2 and then to 4, a sharp increase of the peak load appears together with a sharp drop just after the peak which indicates an initial reluctancy of the initially disperse cracking region against localization. Comparing with the previous figure for the coarse mesh, we see that the results show a clear spurious mesh-dependence for $\beta \geq 2$.

To complete the overview of the results, Fig 11 displays the cracking patterns for the for the finer mesh and the combinations of α and β discussed in the previous paragraph. The displayed cracks correspond to the last step of the computations ($w_B = 0.1$ mm). The white dashed lines indicates, for each case, the central cross-section of the specimen; the arrows at the top of these lines represent the residual loading force at the mid-point. Note that in the right-most image, which corresponds to $\beta = 4$, the crack is far from vertical, and that its mouth is far away from the mid-plane; note also the large bulb of diffuse cracking around the crack tip in this case.

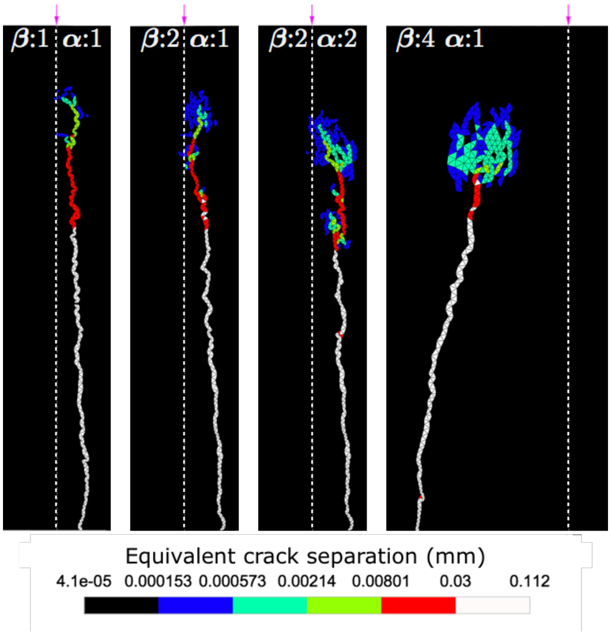

Figure 11: Cracking pattern at the end of the last step (mid-span elongation $w_B = 0.1$ mm) for the finer mesh and various combinations of α and β. A central slice of each specimen is drawn; the central section is marked by a white dashed line and by the upper arrow which represents the residual loading force.

5 CONCLUSIONS

From the foregoing theoretical and numerical results we can draw the following conclusions:

1. A damage-based model has been presented that is defined by equations (5) and (6), which includes and extends most of the models of this type found in the literature.

2. The *shear energy factor* α controls the ratio between the fracture energies in modes II and I according with Eq. (8), and does not introduce spurious behaviors in the analysis of the growth of a crack in, nominally, Mode I.

3. The *shear stiffness factor*, on the contrary, do introduce serious spurious disturbances in the computational results. This suggests that, until a deeper analysis might prove the contrary, the best choice is to take $\beta = 1$ which guarantees coaxiality of traction and separation vectors and, therefore, frame-indifference of the fracture power and rotational equilibrium of cohesive forces.

4. Notwithstanding this, further studies will be carried out to ascertain the influence of β in its low-value range ($\beta < 1.5$, say).

REFERENCES

[1] Hillerborg, A., Modéer, M., and Petersson, P.E., 1976. Analysis of crack formation and crack growth in concrete by means of fracture mechanics and finite elements. *Cement and Concrete Research* **6**:773–781.

[2] Elices, M. and Planas, J., 1989. Material models, chapter 3, in L. Elfgren (Ed.), *Fracture Mechanics of Concrete Structures*, pp. 16–66, Chapman & Hall, London.

[3] Bažant, Z.P. and Planas, J., 1998. *Fracture and Size Effect in Concrete and Other Quasibrittle Materials*, CRC Press, Boca Raton, FL.

[4] Elices, M., Guinea, G.V., Gómez, J., and Planas, J., 2002. The cohesive zone model: advantages, limitations and challenges. *Engineering Fracture Mechanics* **69**:137–163.

[5] Planas, J., Elices, M., Guinea, G.V., Gomez, F.J., Cendon, D.A., and Arbilla, I., 2003. Generalizations and specializations of cohesive crack models. *Engineering Fracture Mechanics* **70**:1759–1776.

[6] Park, K. and Paulino, G.H., 2013. Cohesive zone models: A critical review of traction-separation relationships across

fracture surfaces. *Applied Mechanics Reviews* **64**:060802–060802–20.

[7] Carol, I., Prat, P.C., and López, C.M., 1997. Normal/shear cracking model: Application to discrete crack analysis. *Journal of Engineering Mechanics* **123**:765–773.

[8] Ohlsson, U. and Olofsson, T., 1997. Mixed-mode fracture and anchor bolts in concrete analysis with inner softening bands. *Journal of Engineering Mechanics* **123**:1027–1033.

[9] Červenka, J., Kishen, J.M.C., and Saouma, V.E., 1998. Mixed mode fracture of cementitious bimaterial interfaces: ; part ii: numerical simulation. *Engineering Fracture Mechanics* **60**:95–107.

[10] Jirásek, M., 2000. Conditions of uniqueness for finite elements with embedded cracks, in *European Congress on Computational Methods in Applied Sciences and Engineering ECCOMAS Barcelona*, pp. 1–19.

[11] Wells, G.N., 2001. *Discontinuous modelling of strain localisation and failure*, Ph.D. thesis.

[12] Alfaiate, J., Wells, G.N., and Sluys, L.J., 2002. On the use of embedded discontinuity elements with crack path continuity for mode-i and mixed-mode fracture. *Engineering Fracture Mechanics* **69**:661–686.

[13] Gálvez, J.C., Červenka, J., Cendón, D.A., and Saouma, V., 2002. A discrete crack approach to normal/shear cracking of concrete. *Cement and Concrete Research* **32**:1567–1585.

[14] Camacho, G.T. and Ortiz, M., 1996. Computational modelling of impact damage in brittle materials. *International Journal of Solids and Structures* **33**:2899–2938.

[15] Pandolfi, A., Krysl, P., and Ortiz, M., 1999. Finite element simulation of ring expansion and fragmentation: The capturing of length and time scales through cohesive models of fracture. *International Journal of Fracture* **95**:279–297.

[16] Ortiz, M. and Pandolfi, A., 1999. Finite-deformation irreversible cohesive elements for three-dimensional crack-propagation analysis. *International Journal for Numerical Methods in Engineering* **44**:1267–1282.

[17] Tijssens, M.G.A., Sluys, B.L.J., and van der Giessen, E., 2000. Numerical simulation of quasi-brittle fracture using damaging cohesive surfaces. *European Journal of Mechanics - A/Solids* **19**:761–779.

[18] Gasser, T.C. and Holzapfel, G.A., 2003. Geometrically non-linear and consistently linearized embedded strong discontinuity models for 3d problems with an application to the dissection analysis of soft biological tissues. *Computer Methods in Applied Mechanics and Engineering* **192**:5059–5098.

[19] Gasser, T.C. and Holzapfel, G.A., 2005. Modeling 3d crack propagation in unreinforced concrete using pufem. *Computer Methods in Applied Mechanics and Engineering* **194**:2859–2896.

[20] Mergheim, J. and Steinmann, P., 2006. A geometrically nonlinear fe approach for the simulation of strong and weak discontinuities. *Computer Methods in Applied Mechanics and Engineering* **195**:5037–5052.

[21] Sancho, J.M., Planas, J., Cendon, D.A., Reyes, E., and Galvez, J.C., 2007. An embedded crack model for finite element analysis of concrete fracture. *Engineering Fracture Mechanics* **74**:75–86.

[22] Radulovic, R., Bruhns, O.T., and Mosler, J., 2011. Effective 3d failure simulations

by combining the advantages of embedded strong discontinuity approaches and classical interface elements. *Engineering Fracture Mechanics* **78**:2470–2485.

[23] Ottosen, N.S., Ristinmaa, M., and Mosler, J., 2015. Fundamental physical principles and cohesive zone models at finite displacements –limitations and possibilities. *International Journal of Solids and Structures* **53**:70–79.

[24] Zhan, Y. and Meschke, G., 2017. Adaptive crack modeling with interface solid elements for plain and fiber reinforced concrete structures. *Materials* **10**:771.

[25] Rots, J.G., 1988. *Computational modeling of concrete fracture*, Ph.D. thesis, Delft University of Technology.

[26] Rots, J.G. and Blaauwendraad, J., 1989. Crack models for concrete: Discrete or smeared? fixed, multi-directional or rotating? *Heron* **34**:1–59.

[27] Wells, G.N. and Sluys, L.J., 2001. Three-dimensional embedded discontinuity model for brittle fracture. *International Journal of Solids and Structures* **38**:897–913.

[28] Wells, G.N. and Sluys, L.J., 2001. A new method for modelling cohesive cracks using finite elements. *International Journal for Numerical Methods in Engineering* **50**:2667–2682.

[29] Costanzo, F., 1998. A continuum theory of cohesive zone models: deformation and constitutive equations. *International Journal of Engineering Science* **36**:1763–1792.

[30] Vossen, B.G., Schreurs, P.J.G., van der Sluis, O., and Geers, M.G.D., 2013. On the lack of rotational equilibrium in cohesive zone elements. *Computer Methods in Applied Mechanics and Engineering* **254**:146–153.

[31] Planas, J., Sancho, J.M., and Sanz, B., 2018. *Unified approach to damage-based, traction-separation laws for cohesive cracks in quasibrittle materials*, Technical Report CG-2018-03, Dep. de Ciencia de Materiales, Universidad Politécnica de Madrid.

[32] Lemaitre, J. and Chaboche, J.L., 1985. *Mécanique des Matériaux Solides*, Dunod.

[33] Jirásek, M. and Zimmermann, T., 2001. Embedded crack model: I. basic formulation. *International Journal for Numerical Methods in Engineering* **50**:1269–1290.

[34] Planas, J., Sanz, B., and Sancho, J., 2016. Transition from smeared to localized cracking in macro-defect-free quasibrittle structures. *Procedia Structural Integrity* **2**:3676–3683.

[35] Geuzaine, C. and Remacle, J.F., 2009. Gmsh: A 3-d finite element mesh generator with built-in pre- and post-processing facilities. *International Journal for Numerical Methods in Engineering* **79**:1309–1331.